Warm phase of AMV damps ENSO through weakened thermocline feedback

Paloma Trascasa Castro[1,1], Yohan Ruprich-Robert[2,2], Frederic S. Castruccio[3,3], and Amanda Maycock[1,1]

[1]University of Leeds
[2]Barcelona Supercomputing Center
[3]National Center for Atmospheric Research (NCAR)

September 21, 2021

Abstract

Interactions between ocean basins affect El Niño Southern Oscillation (ENSO), altering its impacts on society. Here, we explore the effect of Atlantic Multidecadal Variability (AMV) on ENSO behaviour using idealized experiments performed with the NCAR-CESM1 model. Comparing warm (AMV+) to cold (AMV-) AMV conditions, we find that ENSO sea surface temperature (SST) anomalies are reduced by ˜10% and ENSO precipitation anomalies are shifted to the west during El Niño and east during La Niña. Using the Bjerknes stability index, we attribute the reduction in ENSO variability to a weakened thermocline feedback in boreal autumn. In AMV+, the Walker circulation and trade winds strengthen over the Pacific, increasing the background zonal SST gradient. Those background changes shift ENSO anomalies westwards, with wind stress anomalies more confined to the West. We suggest the changes in ENSO-wind stress decrease the strength of the thermocline feedback in the East, eventually reducing ENSO growth rate.

Hosted file

`essoar.10508025.2.docx` available at https://authorea.com/users/558402/articles/607617-warm-phase-of-amv-damps-enso-through-weakened-thermocline-feedback

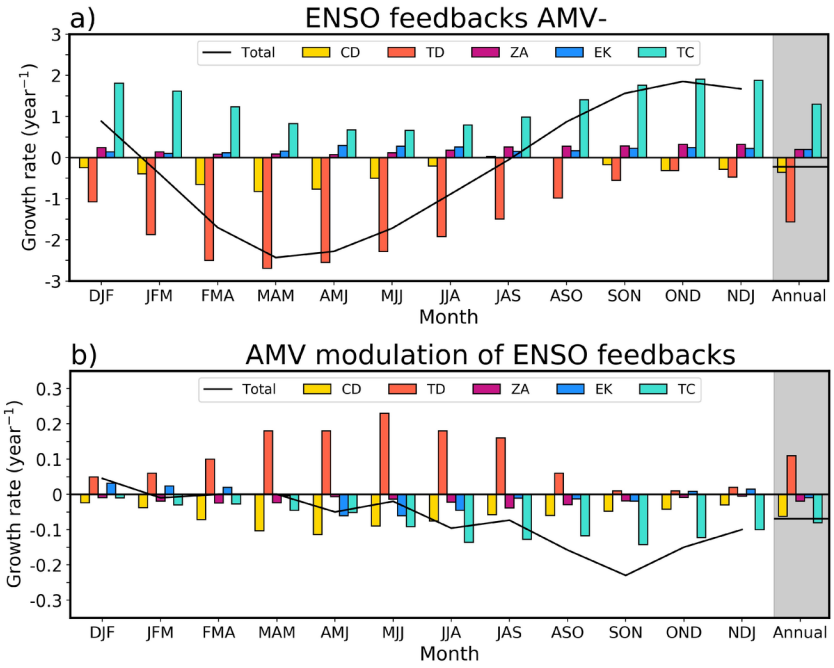

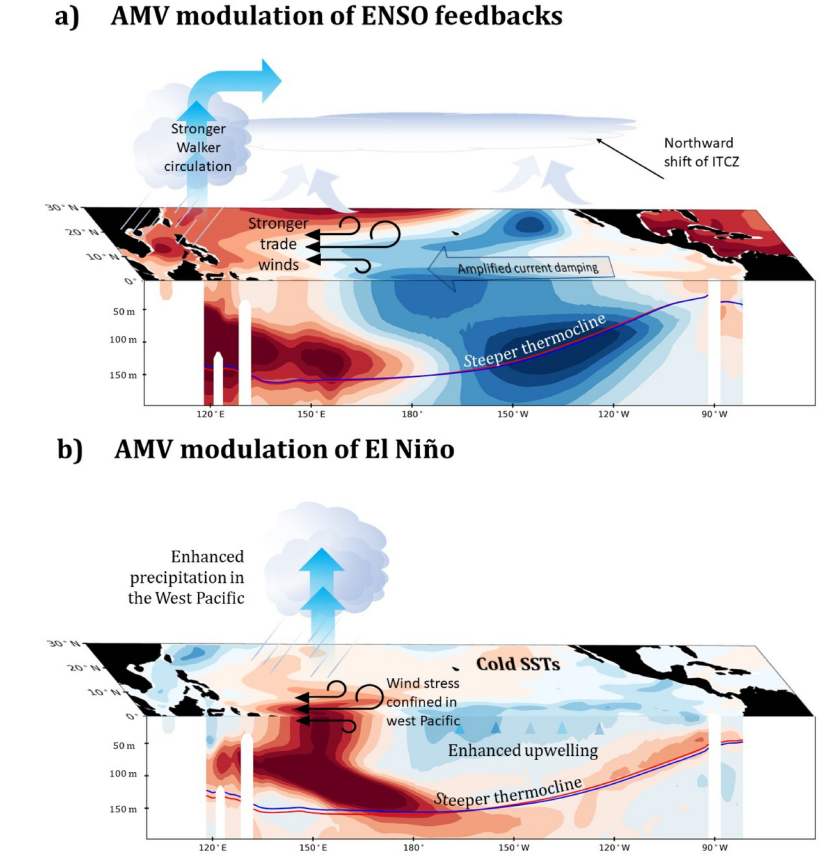

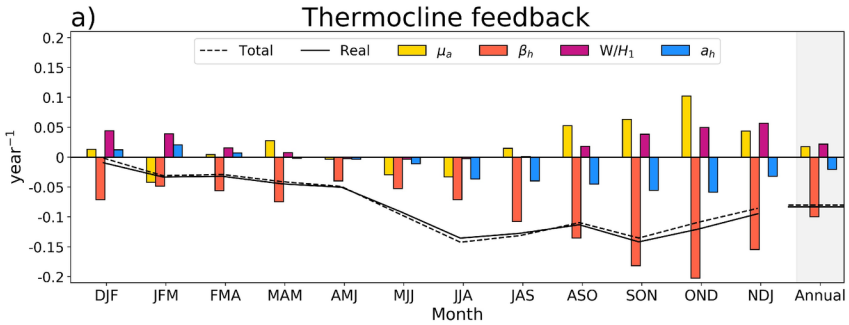

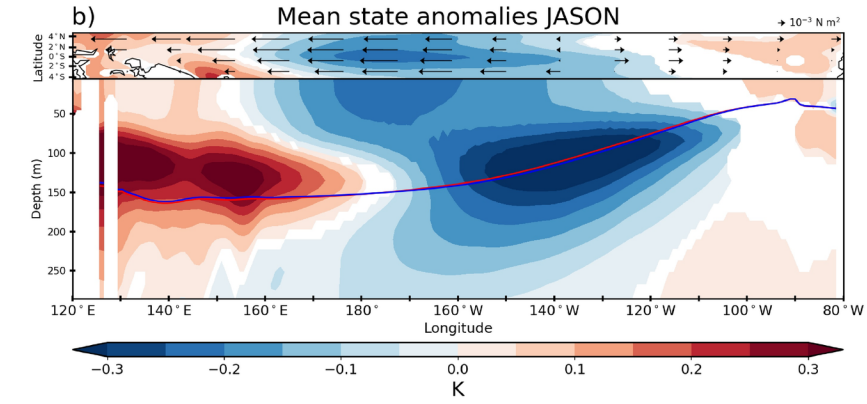

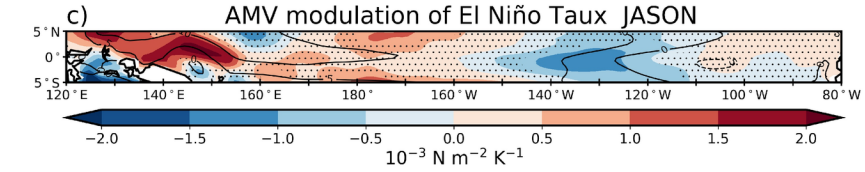

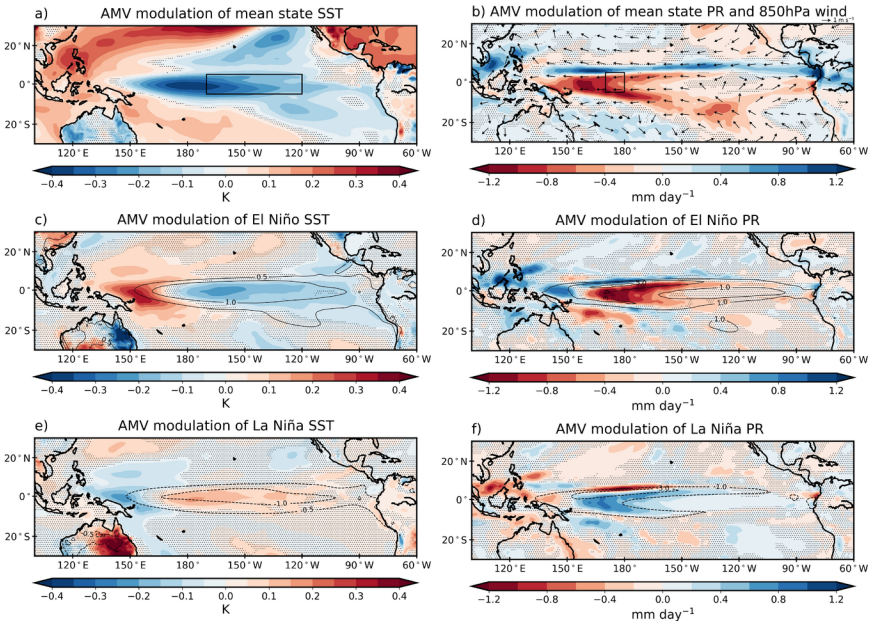

Warm phase of AMV damps ENSO through weakened thermocline feedback

Paloma Trascasa-Castro[1], Yohan Ruprich-Robert[2], Frederic Castruccio[3], Amanda C. Maycock[1]

[1]School of Earth and Environment, University of Leeds, Leeds, UK
[2] Barcelona Supercomputing Center, Barcelona, Spain

[3] National Center for Atmospheric Research, Boulder, CO, USA

Key points:

- AMV weakens ENSO sea surface temperature anomalies by 10% and local ENSO precipitation anomalies by up to 45%
- The thermocline feedback in the tropical Pacific is weakened in boreal autumn, reducing ENSO growth rate
- AMV causes changes in the Pacific mean state that lead to wind stress anomalies being more confined in the west Pacific during ENSO onset

Abstract

Interactions between ocean basins affect El Niño Southern Oscillation (ENSO), altering its impacts on society. Here, we explore the effect of Atlantic Multidecadal Variability (AMV) on ENSO behaviour using idealized experiments performed with the NCAR-CESM1 model. Comparing warm (AMV+) to cold (AMV-) AMV conditions, we find that ENSO sea surface temperature (SST) anomalies are reduced by ~10% and ENSO precipitation anomalies are shifted to the west during El Niño and east during La Niña. Using the Bjerknes stability index, we attribute the reduction in ENSO variability to a weakened thermocline feedback in boreal autumn. In AMV+, the Walker circulation and trade winds strengthen over the tropical Pacific, increasing the background zonal SST gradient. The background changes shift ENSO anomalies westwards, with wind stress anomalies more confined to the West. We suggest the changes in ENSO-wind stress decrease the strength of the thermocline feedback in the East, eventually reducing ENSO growth rate.

Plain language summary

El Niño-Southern Oscillation (ENSO) is the dominant mode of year-to-year climate variability in the tropics and affects regional climates around the world. Understanding the drivers of ENSO behaviour is important for its prediction. One influential factor is communication between ocean basins, such as the North Atlantic interaction with the tropical Pacific. In our work we use idealised simulations that represent the positive and negative phases of the Atlantic Multidecadal Variability (AMV) to understand how sea surface temperature changes in the North Atlantic affect the dynamics of ENSO in the tropical Pacific. We

find that both El Niño and La Niña events are weaker when the North Atlantic is warmer than usual, and vice versa. During the warm phase of the AMV (AMV+), the trade winds associated with the Walker circulation are localised in the west Pacific, directly impacting sea surface temperature patterns associated with ENSO events. Reduced wind stress in the eastern equatorial Pacific means that the upper ocean heat content is less perturbed in the AMV+ simulation, eventually feeding back to ENSO-related sea surface temperatures.

1. Introduction

El Niño Southern Oscillation (ENSO) is the dominant mode of interannual climate variability in the tropics. The spatio-temporal characteristics of ENSO exhibit variations (Wittenberg 2009; Dieppois *et al.* 2021) driven by chaotic atmosphere-ocean dynamics (Fedorov *et al.* 2003; Zhang *et al.* 2021) and sources of variability from outside the tropical Pacific (Meehl *et al.* 2001). Given the global reach of ENSO and its impacts (Diaz *et al.* 2001), understanding and predicting changes in ENSO is a major challenge for the scientific community.

In the last decade, it has become evident that climate variability and changes in other ocean basins can affect the tropical Pacific and ENSO (Cai *et al.* 2019). One example is the impact of Atlantic Multidecadal Variability (AMV) on the mean climate in the tropical Pacific (e.g., Ruprich-Robert *et al.* 2017). However, the extent to which AMV affects ENSO remains unclear (Dong and Sutton 2007; Yu *et al.* 2015; Levine *et al.* 2017; Hu and Fedorov 2018). On interannual timescales, sea surface temperature (SST) anomalies in the tropical North Atlantic alter tropical Pacific SSTs via subtropical teleconnections (Ham and Kug 2015; Wang *et al.* 2017). Warm SST anomalies in the equatorial Atlantic are known to influence ENSO variability by strengthening the Walker circulation (Rodríguez-Fonseca *et al.* 2009; Polo *et al.* 2014). The intensified descending branch in the equatorial east Pacific reinforces the trade winds and supports the development of a La Niña event in the following winter.

Levine *et al.* (2017) found that the AMV alters both the seasonal and annual ENSO stability by changing the mean seasonal cycle in the tropical Pacific. In the relatively short observational record, they found evidence for reduced ENSO growth rate in boreal autumn and winter when the North Atlantic is anomalously warm, but their model experiments did not reproduce this and instead showed the opposite behaviour. Zanchettin *et al.* (2016) identified a delayed response to the AMV in the tropical Pacific and suggested this could contribute to multidecadal ENSO variability. Both Zanchettin *et al.* (2016) and Levine *et al.* (2017) highlight that changes in thermocline dynamics are key to understanding the modulation of ENSO by the AMV. Despite this common finding, owing to the short observational record and different results from model studies there remains uncertainty around the impact of the AMV on ENSO.

This study aims to advance understanding of the processes by which the AMV affects ENSO characteristics using idealised simulations performed with the NCAR-CESM1 climate model. The paper explores changes in the atmospheric

and oceanic processes that are responsible for ENSO growth and decay using the Bjerknes Stability index (hereafter BJ index). With this comprehensive approach, we are able to identify specific mechanisms involved in changes in ENSO under different AMV states.

This paper is laid out as follows: Section 2 describes the model, experimental design and BJ index. The modulation of ENSO behaviour by AMV is detailed in section 3. Our results are discussed in section 4, followed by the final remarks in section 4.

2. Data and methods

2.1 Climate model simulations

Simulations were performed with the NCAR-CESM1(CAM5) model (hereafter CESM1; Kay *et al.* 2015). All components of CESM1 have ~1º horizontal resolution. The atmospheric component CAM5.2 has 30 hybrid vertical levels. The ocean component POP2 has 60 vertical levels and a meridional mesh refinement down to ~0.25º near the equator. CESM1 simulates ENSO in good agreement with observations (Fig. S2, DiNezio *et al.* 2017; Zhang *et al.* 2017; Wu *et al.* 2021).

To assess the impacts of the AMV on ENSO behaviour, idealised experiments were performed in which warm (AMV+) and cold (AMV-) SST anomalies equivalent in amplitude but opposite in sign are imposed in the North Atlantic through surface relaxation (Fig. S1) (Ruprich-Robert *et al.* 2017; Castruccio *et al.* 2019). The imposed SST anomalies do not vary in time nor account for AMV seasonality. The simulations follow the protocol of the Decadal Climate Prediction Project Phase C Idealized AMV experiment (Boer *et al.* 2016), with the minor exception that the observed AMV pattern was computed from the ERSSTv3b (Smith *et al.* 2008) dataset instead of ERSSTv4 (Huang and Xie 2015).

Three ocean initial states are obtained from a preindustrial control simulation; the corresponding atmospheric conditions are perturbed at round-off level in the potential temperature field to obtain 10 different atmospheric initial conditions (Castruccio *et al.* 2019). This produces 30 ensemble members each integrated for 10 years, giving a total of 300 years for each AMV phase. The first 11 months of the simulation are discarded and the analysis presents results from the remaining period.

2.2 Analysis methods

2.2.1 ENSO definition

El Niño and La Niña events are defined when SST anomalies in the Niño3.4 region (5°N-5°S, 170°W-120°W, cf. Figure 1a) exceed ±0.5 K during boreal winter (from December to February, hereafter DJF) relative to the climatology of each simulation. This identifies 77 and 79 El Niños in the AMV+ and AMV-

simulations, respectively. For La Niña, there are 91 events in AMV+ and 103 in AMV-.

To estimate the AMV modulation of ENSO impacts, we first estimate El Niño anomalies with respect to each AMV experiment mean state and then subtract the AMV- El Niño composite from AMV+ the El Niño composite:

$$ENSO\ modulation\ = (El\ Nio_{AMV+}\ -\ \mu_{amv+}) - (El\ Nio_{AMV-}\ - \mu_{AMV-}),$$

(Eq. 1)

where μ_{AMV+} and μ_{AMV-} are time averaged SSTs in the AMV+ and AMV- simulations, respectively. The AMV modulation of La Niña impacts is calculated following the same approach.

2.2.2 The Bjerknes Stability index

To examine the processes underpinning any changes in ENSO characteristics due to the AMV, we use the BJ index introduced by Jin *et al.* (2006), which is proportional to ENSO growth rate. This is based on the recharge oscillator model (Jin 1997) and captures the main atmosphere and ocean processes responsible for ENSO growth and decay (Kim and Jin 2011a). The BJ index has been widely used to compare ENSO behaviour between different climate models (Kim and Jin 2011a; Kim and Jin 2011b), time periods (Lübbecke and Mcphaden 2013) and background states (Levine *et al.* 2017; Ferrett and Collins 2019). The BJ index is defined as:

$$2BJ = -\left[a_1\frac{\langle\,\overline{u}\rangle_E}{L_x} + \ a_2\frac{\langle\,\overline{v}\rangle_E}{L_y}\right]_{\mathrm{CD}} - [\alpha_s]_{\mathrm{TD}} + \left[\mu_a\beta_u\left\langle-\frac{\partial\overline{T}}{\partial x}\right\rangle_E\right]_{\mathrm{ZA}} + \left[\mu_a\beta_w\left\langle-\frac{\partial\overline{T}}{\partial z}\right\rangle_E\right]_{\mathrm{EK}} + \left[\mu_a\beta_h\left\langle-\frac{\overline{w}}{H_1}\right\rangle_E a\right.$$

(Eq. 2)

The ENSO growth rate is estimated as the sum of, from left to right, the current damping (CD), thermodynamic (TD), zonal advective (ZA), Ekman (EK) and thermocline (TC) feedbacks. Following previous studies (Jin *et al.* 2006; Guilyardi *et al.* 2009; Kim and Jin 2011a; Kim and Jin 2011b; Lübbecke and Mcphaden 2013; An *et al.* 2017), the BJ index terms are calculated using linear regression between variables across all years in the simulations. A full description of the equation is given in the Supplementary Information.

The BJ index assumes linearity between variables, and may therefore fail to represent processes that are nonlinear by nature, such as the dependence of shortwave fluxes on SSTs (See Fig. S4) (Lloyd *et al.* 2012; Graham *et al.* 2014). However, as discussed below, we find that for the feedbacks that are responsible for the AMV modulation of ENSO the linear approximation is reasonable to

first order (Fig. S5). Despite certain simplifying assumptions used in the BJ index, it has been widely used and shown to be insightful for understanding ENSO behaviour.

The relative contributions of the individual terms in the feedbacks in Eq. 2 to the modulation of ENSO growth rate are calculated using a delta method where for a given term the difference between AMV+ and AMV- is multiplied by the AMV- value of all the other terms. The delta method applied to the thermocline feedback is as follows:

$$\mu_a = (\mu_{AMV+} - \mu_{AMV-}) \times \beta_{h\,AMV-} \times \frac{\overline{w}}{H_1}_{AMV-} \times \; a_{h_{AMV-}}$$

$$\beta_h = \mu_{AMV-} \times \left(\beta_{h\,AMV+} - \beta_{h\,AMV-}\right) \times \frac{\overline{w}}{H_1}_{AMV-} \times \; a_{h_{AMV-}}$$

$$\frac{\overline{w}}{H_1} = \mu_{AMV-} \times \beta_{h\,AMV-} \times \left(\frac{\overline{w}}{H_1}_{AMV+} - \frac{\overline{w}}{H_1}_{AMV-}\right) \times \; a_{h_{AMV-}}$$

$$a_h = \mu_{AMV-} \times \beta_{h\,AMV-} \times \frac{\overline{w}}{H_1}_{AMV-} \times \left(a_{h_{AMV+}} - a_{h_{AMV-}}\right)$$

$$\sum TC = \; \mu_a + \beta_h + \; \frac{\overline{w}}{H_1} + \; a_h$$

(Eq.3)

Finally, to test whether the difference in ENSO impacts and feedbacks between AMV+ and AMV- are statistically significant at the 95% confidence level, we perform a non-parametric bootstrap test with replacement, subsampling 70% of years on each iteration repeated 10^4 times and where we assume that all years are independent from each other.

3. Results

3.1 AMV modulation of Pacific mean state and ENSO variability

In boreal winter (DJF), warm AMV conditions drive tropical Pacific cooling of -0.23 K in the Niño3.4 region, with a minimum of -0.35 K near the dateline (Fig. 1a). This response is consistent with modelling studies (Dong *et al.* 2006; Zanchettin *et al.* 2016; Ruprich-Robert *et al.* 2017; Ruprich-Robert *et al.* 2018) although CESM1 simulates a stronger tropical Pacific response than some other climate models for similar imposed AMV anomalies (Ruprich-Robert *et al.* 2021). The mean precipitation response to AMV+ (Fig. 1b) shows the Intertropical Convergence Zone (ITCZ) is shifted north in boreal winter, and the South Pacific Convergence Zone (SPCZ) is weakened. These changes in the tropical Pacific mean state are a signature of a strengthened Walker circulation

(Lübbecke and Mcphaden 2013) a key mechanism in the tropical Pacific response to warm SSTs in the tropical Atlantic at any timescale (Meehl *et al.* 2011; Kosaka and Xie 2013; Ham and Kug 2015; Ruprich-Robert *et al.* 2017).

In DJF, AMV+ damps ENSO variability, reducing the magnitude of SST and precipitation anomalies in both El Niño and La Niña phases (Figs. 1c and 1e). El Niño events in AMV+ have, on average, cooler SSTs in the central and eastern equatorial Pacific (hereafter EP), and relatively warmer SSTs in the west Pacific, as compared to AMV-. The Niño3.4 SST difference between AMV+ and AMV- is -0.17 K (13%). The modulation of La Niña SSTs by the AMV has a similar pattern with opposite sign and a slightly smaller amplitude: the La Niña composite Niño3.4 SST is 0.09 K (9%) warmer in AMV+. Hence, in CESM1 AMV modulates the amplitude of ENSO SST anomalies by around 10% in the Niño3.4 region.

The AMV modulation of ENSO SSTs is accompanied by modulation of precipitation anomalies in the equatorial Pacific. During AMV+, the area of maximum anomalous precipitation associated with El Niño shifts from the central to the western Pacific, with a reduction in precipitation anomaly of up to 1.15 mm day^{-1} around the equator and between 170°E and 180° (Fig. 1d) and an increase in precipitation anomalies over the warm pool and Maritime continent. This represents a statistically significant decrease in the central Pacific precipitation anomaly under El Niño by ~40% (see box in Fig. 1b) as compared to AMV-. AMV modulates the precipitation response to La Niña in a similar way (Fig. 1f). In this case, during AMV+ the precipitation anomaly decreases in the western equatorial Pacific and increases over the central Pacific by 0.65 mm day^{-1} (45%). Hence, in CESM1 the modulation by AMV of ENSO precipitation is proportionately larger than for SSTs. This can be explained by the non-linear relationship between precipitation and SST in the Niño3.4 region. To test this non-linearity, a simple regression model was built considering only El Niño events. This model shows that around 90% of the El Niño precipitation modulation by AMV can be explained by the SST modulation (not shown). Hence, the modulation by AMV of ENSO SST signal is of leading importance for the modulation of ENSO atmospheric response.

The decrease in ENSO variability simulated by CESM1 in AMV+ is consistent with observations (Lübbecke and Mcphaden 2014; Zanchettin *et al.* 2016; Levine *et al.* 2017). Our results are also consistent with the modelling study of Dong et al. (2006), but opposite to the ones of Levine et al. (Levine *et al.* 2017). To further understand the modulation of ENSO by AMV, we next investigate the physical processes driving this modulation using the BJ index (cf. Section 2.2.2).

3.2 AMV modulation of ENSO feedbacks

CESM1 simulates a realistic seasonal cycle of ENSO growth rate in the reference AMV- simulation (Fig. 2a), with a minimum of ~-2.4 year^{-1} in spring and a maximum of ~1.7 year^{-1} in autumn (cf. solid black line). Maximum values of

the BJ index in October-November-December coincide with the development and growth of ENSO events, whereas minimum values are reached in March-April-May, when ENSO decays. On average over the year, the ENSO growth rate simulated by CESM1 is -0.22 year^{-1}, which is very close to reanalysis-based estimates of -0.24 year^{-1} (Kim *et al.* 2014). The annual growth rate depends on the balance between positive and negative feedbacks. The negative sign of the annual mean BJ index is dominated by the damping of SST anomalies by the thermodynamic feedback, peaking in early spring, which is composed of the sum of the surface heat fluxes. The thermocline feedback peaking in late fall is the main process that intensifies ENSO anomalies (Jin *et al.* 2020).

Consistent with the damped ENSO variability seen in Fig. 1, AMV+ leads to a more negative annual mean ENSO growth rate by -0.07 year^{-1} (Fig. 2b), which represents a ~30% decrease in magnitude compared to AMV-. The main contributions to the decreased annual ENSO growth rate in AMV+ are a weakened thermocline feedback (-0.08 year^{-1}) and a stronger current damping feedback (-0.06 year^{-1}) (Fig. 2b). These changes are partly offset by a weakened (i.e. reduced damping) thermodynamic feedback by 0.1 year^{-1}. There are negligible changes in the Ekman feedback and zonal advective feedback due to AMV (see also Fig. S3) and these will not be discussed further.

The AMV modulation of the thermodynamic feedback is strongest in boreal summer, contributing to an increase in growth rate of up to 0.23 year^{-1} in May-June-July. Of the two terms contributing to a reduced ENSO growth rate, the modulation of the current damping peaks in April-May-June. The modulation of the thermocline feedback by AMV dominates from boreal summer through early winter (JJA to NDJ) and therefore has a particular influence during the ENSO growth season. This suggests the thermocline feedback is an important driver of the changes in ENSO behaviour between AMV+ and AMV-.

Investigation of the contributions of individual terms in Eq. 2 to the overall modulation of the BJ index feedbacks (Fig. S3) reveals that the modulation of most terms is not strongly statistically significant. The main exception which is relevant to understanding the dampening of ENSO by AMV+ is the thermocline feedback, which is dominated by a statistically significant decrease in the magnitude of the regression between equatorial Pacific wind stress anomalies and the thermocline slope ($_{h}$ in Eqn 2, orange bar Fig. 3a). This leads to a reduction in ENSO growth rate by 0.1 year^{-1}. The finding that the AMV modulates ENSO through modifying how the thermocline slope responds to equatorial Pacific wind stress anomalies is in agreement with Zanchettin et al. (2016). We discuss in the following section how the AMV impacts on the equatorial Pacific mean state alters this relationship.

4. Discussion

A mean tropical Pacific cooling in response to a tropical Atlantic warming is well documented in the literature (Fig. 4a). Warm tropical Atlantic SST anomalies intensify deep convection and lead to upper tropospheric mass divergence over

the tropical Atlantic, which modifies the entire Walker Circulation (Dong and Sutton 2007; Rodríguez-Fonseca *et al.* 2009; Martin-Rey *et al.* 2014; McGregor *et al.* 2014; Polo *et al.* 2014; Ham and Kug 2015; Zanchettin *et al.* 2016; Ruprich-Robert *et al.* 2017; Ruprich-Robert *et al.* 2021). This is associated with an intensification of the trade winds, which deepens the thermocline in the west Pacific and steepens the thermocline slope (Fig. 3b; Kucharski *et al.* 2014; Polo *et al.* 2014; Meehl *et al.* 2021).

Differences in the mean state between AMV+ and AMV- damp ENSO in CESM1 mainly by a weakened thermocline feedback. The weaker thermocline slope sensitivity to equatorial Pacific wind stress (i.e. smaller $_{h}$) can be explained by a decrease in ocean stratification associated with a deepening of the thermocline (Zebiak and Cane 1987; Jin and An 1999) and/or a change in the wind stress forcing pattern (Kang and Kug 2002; Wang and An 2002; Choi *et al.* 2011). Dong *et al.* (2006) found that intensified trade winds during AMV+ led to a deepened thermocline in the western and central tropical Pacific. They argue that this deepening reduces the development of sub-surface temperature anomalies in response to wind stress (Zebiak and Cane 1987), which eventually weakens ENSO. We also find the thermocline deepens by 0.6 m on average in the western tropical Pacific from late summer to early winter in AMV+ (Fig. 3b). Conversely, the thermocline shallows by 0.7 m over the central and eastern equatorial Pacific, which following this logic would increase its sensitivity to wind stress anomalies. The climatological thermocline in this region is shallower than over the western Pacific and therefore potentially more responsive to wind anomalies (Castaño-Tierno *et al.* 2018). The shallowing of the thermocline in the central and eastern equatorial Pacific would therefore lead to an increase in $_{h}$. Thus, we conclude this mechanism cannot explain the ENSO response in our simulations.

Regarding the second mechanism, we find the pattern of wind stress anomalies associated with ENSO is modulated by AMV (Fig. 3c). During AMV+, equatorial wind stress anomalies are stronger over the western Pacific but extend less to the east (between 150°W and 120°W), where the thermocline is shallower and therefore more sensitive to wind stress (Castaño-Tierno *et al.* 2018). We suggest this weakening of ENSO-wind stress anomalies in the region where the thermocline is more sensitive to wind forcing can explain the $_{h}$ decrease in AMV+. This conclusion aligns with previous studies that also find a reduction in ENSO variance associated with a steeper thermocline mean state in the equatorial Pacific (Fedorov and Philander 2000; Lübbecke and Mcphaden 2014; Hu and Fedorov 2018).

Following Lubbecke and McPhaden (2014), we argue that the decrease of the ENSO-wind forcing over the eastern Pacific in AMV+ is linked to a strengthening of the climatological zonal SST gradient (Fig. 3b). Associated with the stronger zonal SST gradient in the tropical Pacific, the warmest SSTs are shifted westward compared to AMV-. The response of deep convection to SST anomalies in the tropics is a function of the climatological SST, with stronger

precipitation responses over climatologically warm SSTs (Graham and Barnett 1987), so the ENSO-precipitation and associated wind convergence anomalies are also expected to shift westward in AMV+.

With a similar experimental design but a different model, Levine *et al.* (2017) found that AMV+ increases ENSO growth rate and amplitude, in contrast to the modulation apparent in observations and found in our simulations. They suggest this discrepancy comes from a too sensitive thermocline feedback to SST anomalies in the eastern tropical Pacific in their model (Kim and Jin 2011a). Nevertheless, this difference in behaviour of models calls for a multi-model analysis, which will be conducted in a future study using the AMV idealized experiments performed within the Component C of the Decadal Climate Prediction Project (Boer *et al.* 2016).

5. Conclusions

We have used idealized ensemble simulations with the CESM1 model where North Atlantic SSTs are restored towards observed warm (AMV+) and cold (AMV-) AMV states to investigate its impact on ENSO variability. Comparing AMV+ to AMV-, we find that warm North Atlantic conditions reduce the amplitude of SST anomalies associated with ENSO by around 10% in both El Niño and La Niña phases. ENSO precipitation anomalies decrease by a larger proportion of up to 45%. During AMV+, the trade wind slackening associated with El Niño are more confined to the west and are accompanied by a westward shift of the maximum SST and deep convection anomalies (Fig. 4b).

Using the BJ index as a proxy for ENSO growth rate, we find that the decrease of ENSO variance under AMV+ conditions comes mainly from a decrease in the thermocline feedback in AMV+ and, to a smaller extent, by a decrease of the current damping feedback. We hypothesise that the decrease of the thermocline feedback in AMV+ results from the strengthened trade winds localised over the western equatorial Pacific, and associated steepening of the background thermocline, which increase the east-west mean SST gradient in the equatorial Pacific. In the equatorial east Pacific, climatological zonal ocean currents are weaker during boreal autumn in AMV+ compared to AMV-, as is the zonal SST gradient. During El Niño events, this increased zonal SST gradient prevents the convection and westerlies anomalies from propagating through the east where the thermocline is shallower and therefore more responsive to wind stress anomalies. It results in a weakening of the wind-thermocline relationship, which eventually reduces ENSO growth rate.

Our results show a substantial modulation of ENSO by AMV in the CESM1 model. The AMV modulation of ENSO growth rate is opposite to the projected changes under global warming (Collins *et al.* 2010). Decadal climate variability may therefore mask or amplify the signature of anthropogenic climate change and must be accounted for in future ENSO predictions. Changes to ENSO SST and precipitation variability are likely to have extratropical implications. Further work will explore the role of the AMV in the modulation of ENSO

extratropical impacts and their variability.

Acknowledgements

P.T.-C. was supported by a PhD scholarship from the Natural Environment Research Council PANORAMA Doctoral Training Partnership (NE/S007458/1). Y.R.-R. was funded by the European Union's Horizon 2020 Research and Innovation Program in the framework of the Marie Skłodowska-Curie grant INADEC (Grant agreement 800154). A.C.M. was supported by the European Union's Horizon 2020 research and innovation programme under grant agreement No 820829 (CONSTRAIN project), by a NERC Independent Research Fellowship (NE/M018199/1) and The Leverhulme Trust (PLP-2018-278). F.C was supported by the US National Science Foundation (NSF) under the Collaborative Research EaSM2 Grant OCE-1243015 to NCAR and by the US National Oceanic and Atmospheric Administration (NOAA) Climate Program Office under the Climate Variability and Predictability Program Grant NA13OAR4310138. Computing facilities were provided by the Barcelona Supercomputing Center and the University of Leeds. We thank Dr. Gokhan Danabasoglu for his comments on an earlier version of this manuscript.

Open research

Data from the AMV idealized experiments performed with the NCAR-CESM1 model can be found at the Climate Data Gateway (NCAR): https://doi.org/10.26024/rn3t-ep30.

Figures

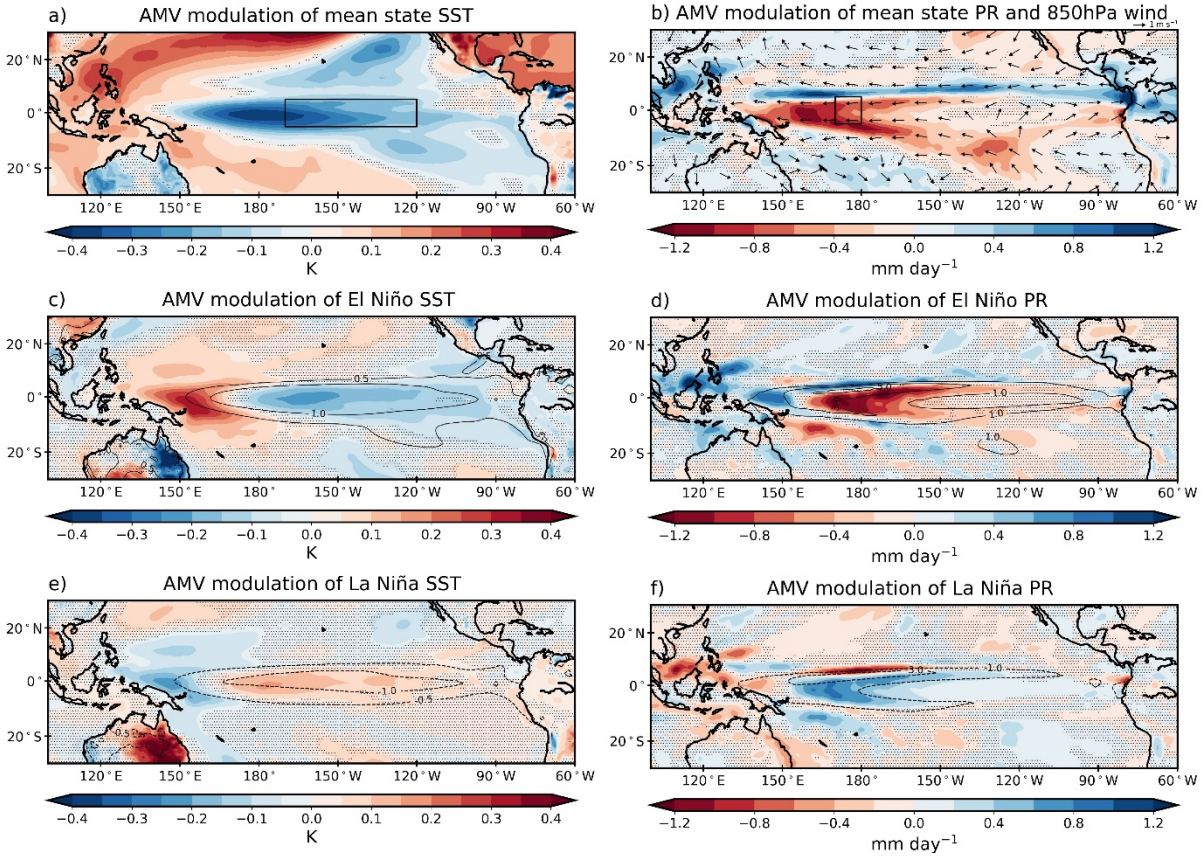

Figure 1. Anomalies for boreal winter (DJF). (top) Tropical Pacific mean state changes between AMV+ and AMV- in (a) SST and (b) precipitation and 850hPa winds. (middle) AMV modulation of El Niño (c) SST and (d) precipitation (shading); composite El Niño anomalies from AMV- overlaid in contours. (bottom) As in middle, but for La Niña. Black boxes in a) and b) denote the Niño3.4 region and the region used for the precipitation index, respectively. Note inverted color bars in the left and right columns. Stippling means not significance at the 95% confidence level.

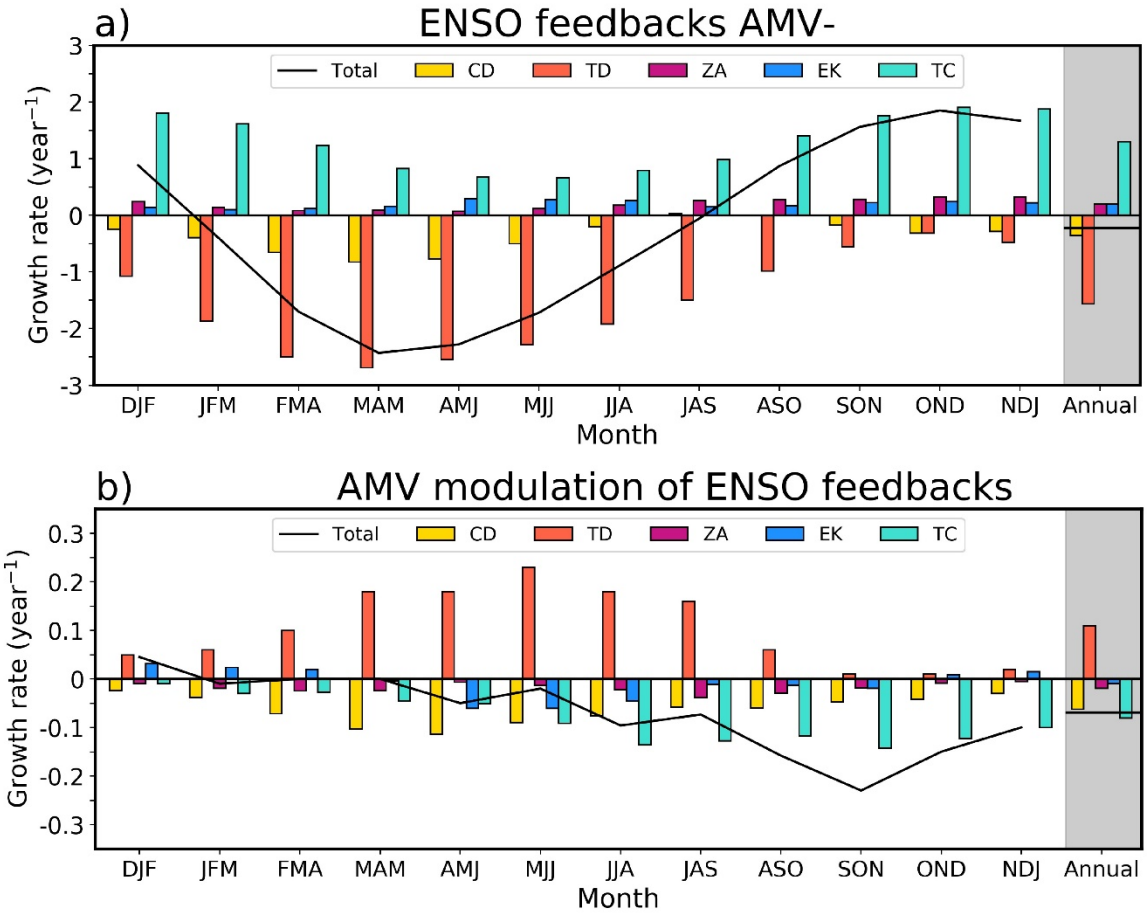

Figure 2: Annual cycle of ENSO feedbacks expressed as growth rate (year^{-1}) in (a) the AMV- simulation, and (b) the difference between AMV+ and AMV-. Monthly values are smoothed with a 3-month running mean. Feedbacks are: current damping (CD, yellow), thermodynamic (TD, orange), zonal advective (ZA, magenta), Ekman (EK, dark blue) and thermocline (TC, light blue). The solid line denotes the total BJ index.

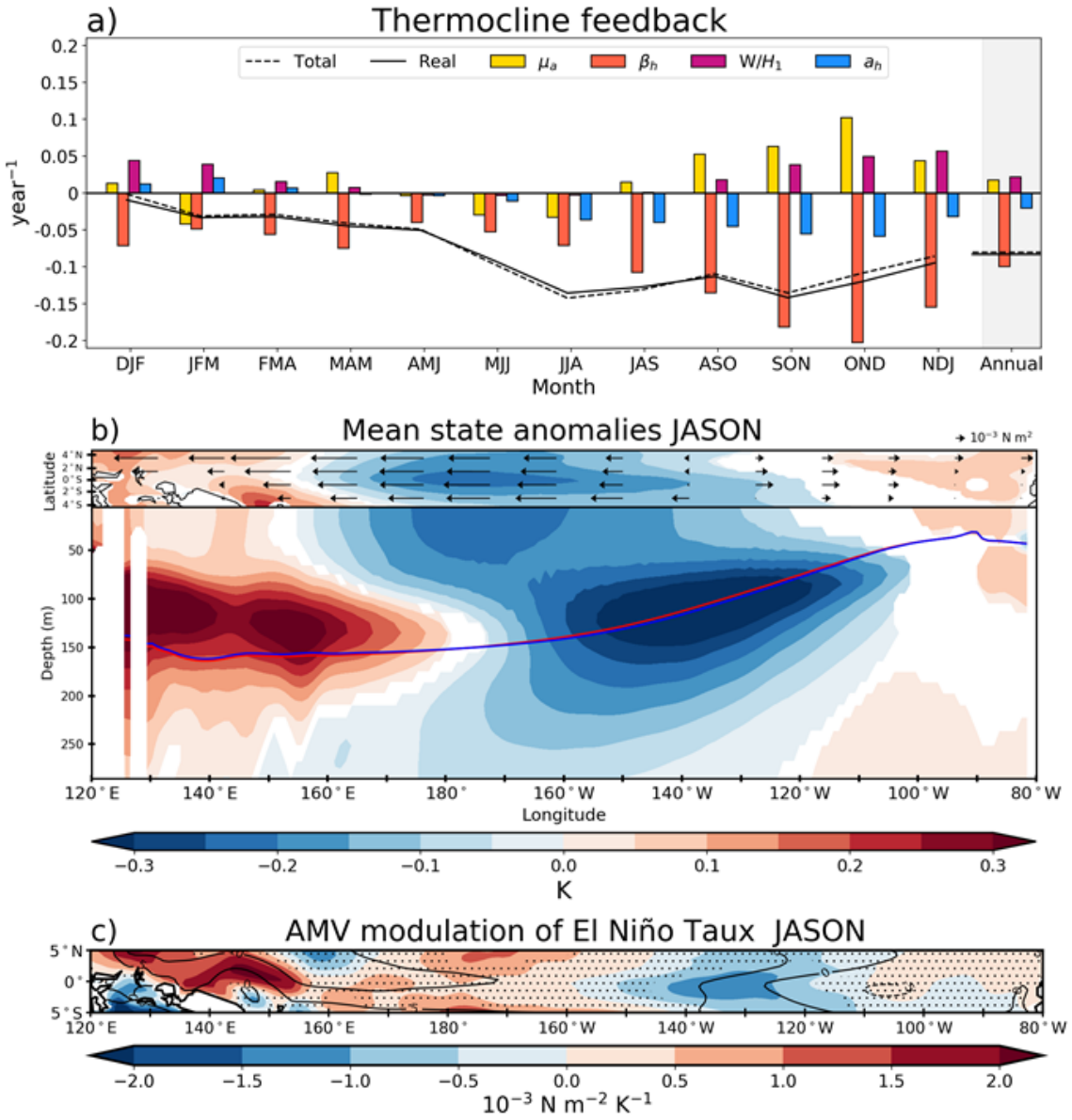

Figure 3. a) AMV modulation of the thermocline feedback and contributions from individual terms. b) 3-dimensional mean state ocean temperature differences (AMV+ minus AMV-) in the equatorial Pacific in JASON. White areas cover non-significant anomalies at the 95% confidence level. Top: Arrows are zonal wind stress anomalies, bottom: Red and blue lines show depth of 20°C isotherm in the AMV+ and AMV- states, respectively. c) AMV modulation of equatorial wind stress in the JASON season prior to El Niño events. Anomalies

are normalised by the mean Niño3.4 SST amplitude in AMV+ and AMV-, respectively. Black contours show wind stress anomalies in the AMV- simulation. Dotted areas show non-significant anomalies at the 95% confidence level.

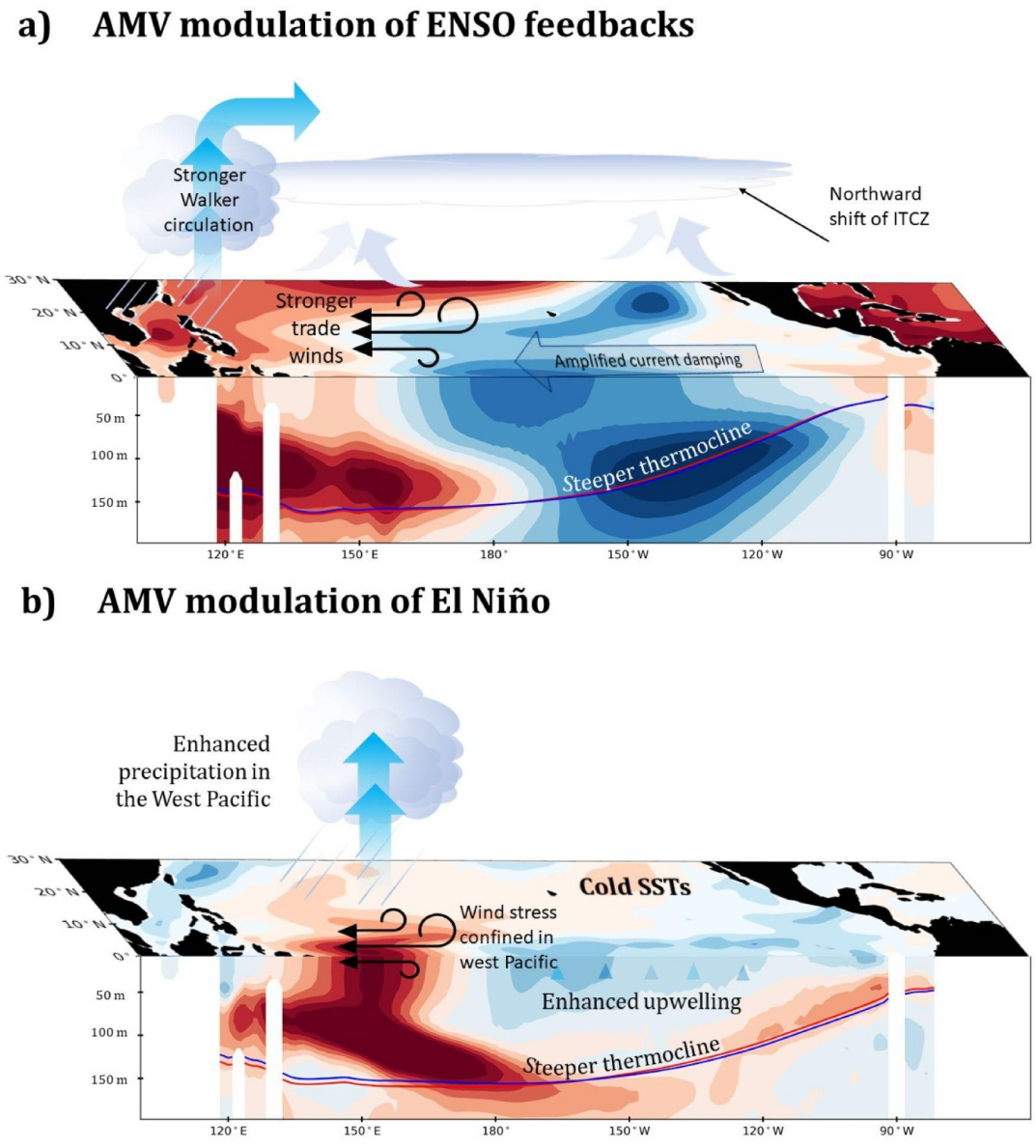

Figure 4. Schematic overlay of a) the mean state changes due to AMV in the equatorial Pacific in JASON, b) the climate response to El Niño modulated

by the AMV in DJF. Shading shows ocean temperature anomalies. Red and blue lines in both panels show the 20°C isotherm in the AMV+ and AMV- experiments, respectively.

References

http://dx.doi.org/10.1002/joc.631.abs

http://dx.doi.org/10.21203/RS.3.RS-387048/V1

http://dx.doi.org/10.1175/jcli-d-16-0127.1

http://dx.doi.org/10.1038/nclimate3351

An, S.I., Heo, E.S. and Kim, S.T. (2017) 'Feedback process responsible for intermodel diversity of ENSO variability', *Geophysical Research Letters*, 44, 4272-4279.Boer, G.J., Smith, D.M., Cassou, C., Doblas-Reyes, F., Danabasoglu, G., Kirtman, B., Kushnir, Y., Kimoto, M., Meehl, G.A., Msadek, R., Mueller, W.A., Taylor, K.E., Zwiers, F., Rixen, M., Ruprich-Robert, Y. and Eade, R. (2016) 'The Decadal Climate Prediction Project (DCPP) contribution to CMIP6', *Geoscientific Model Development*, 9, 3751-3777.Cai, W., Wu, L., Lengaigne, M., Li, T., McGregor, S., Kug, J.S., Yu, J.Y., Stuecker, M.F., Santoso, A., Li, X., Ham, Y.G., Chikamoto, Y., Ng, B., McPhaden, M.J., Du, Y., Dommenget, D., Jia, F., Kajtar, J.B., Keenlyside, N., Lin, X., Luo, J.J., Martín-Rey, M., Ruprich-Robert, Y., Wang, G., Xie, S.P., Yang, Y., Kang, S.M., Choi, J.Y., Gan, B., Kim, G.I., Kim, C.E., Kim, S., Kim, J.H. and Chang, P. (2019) 'Pantropical climate interactions', *Science*, 363.Castaño-Tierno, A., Mohino, E., Rodríguez-Fonseca, B. and Losada, T. (2018) 'Revisiting the CMIP5 thermocline in the equatorial Pacific and Atlantic Oceans', *Geophysical Research Letters*, 45(23), 12,963-12,971.Castruccio, F.S., Ruprich-Robert, Y., Yeager, S.G., Danabasoglu, G., Msadek, R. and Delworth, T.L. (2019) 'Modulation of Arctic sea ice loss by atmospheric teleconnections from Atlantic multidecadal variability', *Journal of Climate*, 32(5), 1419-1441.Choi, J., An, S.-I., Kug, J.-S. and Yeh, S.-W. (2011) 'The role of mean state on changes in El Niño's flavor', *Climate Dynamics*, 37(5), 1205-1215.Collins, M., An, S.-I., Cai, W., Ganachaud, A., Guilyardi, E., Jin, F.-F., Jochum, M., Lengaigne, M., Power, S., Timmermann, A., Vecchi, G. and Wittenberg, A. (2010) 'The impact of global warming on the tropical Pacific Ocean and El Niño', *Nature Geoscience*, 3, 391-397.Diaz, H.F., Hoerling, M.P. and Eischeid, J.K. (2001) 'ENSO variability, teleconnections and climate change', *International Journal of Climatology*, 21(15), 1845-1862, available: .Dieppois, B., Capotondi, A., Pohl, B., Pan Chun, K., Monerie, A. and Eden, J. (2021) 'Robust Decadal Variations in ENSO Diversity, and its Impact on Future Scenarios 2', in, available: .DiNezio, P.N., Deser, C., Okumura, Y. and Karspeck, A. (2017) 'Predictability of 2-year La Niña events in a coupled general circulation model', *Climate dynamics*, 49(11), 4237-4261.Dong, B. and Sutton, R.T. (2007) 'Enhancement of ENSO variability by a weakened Atlantic thermohaline circulation in a coupled GCM', *Journal of Climate*, 20(19),

4920-4939.Dong, B., Sutton, R.T. and Scaife, A.A. (2006) 'Multidecadal modulation of El Niño–Southern Oscillation (ENSO) variance by Atlantic Ocean sea surface temperatures', *Geophysical Research Letters*, 33, L08705.Fedorov, A., Harper, S., Philander, S., Winter, B. and Wittenberg, A. (2003) 'How predictable is El Niño?', *Bulletin of the American Meteorological Society*, 84(7), 911-920.Fedorov, A.V. and Philander, S.G. (2000) 'Is El Nino changing?', *Science (New York, N.Y.)*, 288, 1997-2002.Ferrett, S. and Collins, M. (2019) 'ENSO feedbacks and their relationships with the mean state in a flux adjusted ensemble', *Climate Dynamics*, 52, 7189-7208.Graham, F.S., Brown, J.N., Langlais, C., Marsland, S.J., Wittenberg, A.T. and Holbrook, N.J. (2014) 'Effectiveness of the Bjerknes stability index in representing ocean dynamics', *Climate Dynamics*, 43, 2399-2414.Graham, N. and Barnett, T. (1987) 'Sea surface temperature, surface wind divergence, and convection over tropical oceans', *Science*, 238(4827), 657-659.Guilyardi, E., Braconnot, P., Jin, F.F., Kim, S.T., Kolasinski, M., Li, T. and Musat, I. (2009) 'Atmosphere feedbacks during ENSO in a coupled GCM with a modified atmospheric convection scheme', *Journal of Climate*, 22, 5698-5718.Ham, Y.-G. and Kug, J.-S. (2015) 'Role of north tropical atlantic SST on the ENSO simulated using CMIP3 and CMIP5 models', *Climate Dynamics*, 45, 3103-3117.*Cross-equatorial winds control El Niño diversity and change 2018*, No.8, Nature Publishing Group.Huang, P. and Xie, S.P. (2015) 'Mechanisms of change in ENSO-induced tropical Pacific rainfall variability in a warming climate', *Nature Geoscience*, 8, 922-926.Jin, F.-F. (1997) 'An Equatorial Ocean Recharge Paradigm for ENSO. Part I: Conceptual Model', *Journal of the Atmospheric Sciences*, 54, 811-829.Jin, F.-F. and An, S.-I. (1999) 'Thermocline and Zonal Advective Feedbacks Within the Equatorial Ocean Recharge Oscillator Model for ENSO', *Geophysical Research Letters*, 26, 2989-2992.Jin, F.F., Chen, H.C., Zhao, S., Hayashi, M., Karamperidou, C., Stuecker, M.F., Xie, R. and Geng, L. (2020) 'Simple ENSO models', *El Niño Southern Oscillation in a Changing Climate*, 119-151.Jin, F.F., Kim, S.T. and Bejarano, L. (2006) 'A coupled-stability index for ENSO', *Geophysical Research Letters*, 33.Kang, I.S. and Kug, J.S. (2002) 'El Niño and La Niña sea surface temperature anomalies: Asymmetry characteristics associated with their wind stress anomalies', *Journal of Geophysical Research: Atmospheres*, 107(D19), ACL 1-1-ACL 1-10.Kay, J.E., Deser, C., Phillips, A., Mai, A., Hannay, C., Strand, G., Arblaster, J.M., Bates, S., Danabasoglu, G. and Edwards, J. (2015) 'The Community Earth System Model (CESM) large ensemble project: A community resource for studying climate change in the presence of internal climate variability', *Bulletin of the American Meteorological Society*, 96(8), 1333-1349.Kim, S.T., Cai, W., Jin, F.F. and Yu, J.Y. (2014) 'ENSO stability in coupled climate models and its association with mean state', *Climate Dynamics*, 42, 3313-3321.Kim, S.T. and Jin, F.F. (2011a) 'An ENSO stability analysis. Part I: Results from a hybrid coupled model', *Climate Dynamics*, 36, 1593-1607.Kim, S.T. and Jin, F.F. (2011b) 'An ENSO stability analysis. Part II: Results from the twentieth and twenty-first century simulations of the CMIP3 models', *Climate Dynamics*, 36, 1609-1627.Kosaka, Y. and Xie, S.-P. (2013) 'Recent global-warming hiatus tied to equatorial Pacific surface cooling', *Nature*, 501, 403-407.Kucharski, F., Syed,

F.S., Burhan, A., Farah, I. and Gohar, A. (2014) 'Tropical Atlantic influence on Pacific variability and mean state in the twentieth century in observations and CMIP5', *Climate Dynamics*, 44, 881-896.Levine, A.F.Z., McPhaden, M.J. and Frierson, D.M.W. (2017) 'The impact of the AMO on multidecadal ENSO variability', *Geophysical Research Letters*, 44, 3877-3886.Lloyd, J., Guilyardi, E. and Weller, H. (2011) 'The role of atmosphere feedbacks during ENSO in the CMIP3 models. Part II: using AMIP runs to understand the heat flux feedback mechanisms'.Lloyd, J., Guilyardi, E. and Weller, H. (2012) 'The role of atmosphere feedbacks during ENSO in the CMIP3 models. Part III: the shortwave flux feedback'.Lloyd, J., Guilyardi, E., Weller, H. and Slingo, J. (2009) 'The role of atmosphere feedbacks during ENSO in the CMIP3 models', *Atmospheric Science Letters*, 10, 170-176.Lübbecke, J.F. and Mcphaden, M.J. (2013) 'A comparative stability analysis of atlantic and pacific niño modes', *Journal of Climate*, 26, 5965-5980.Lübbecke, J.F. and Mcphaden, M.J. (2014) 'Assessing the twenty-first-century shift in enso variability in terms of the bjerknes stability index', *Journal of Climate*, 27, 2577-2587.Martin-Rey, M., Rodriguez-Fonseca, B., Polo, I. and Kucharski, F. (2014) 'On the Atlantic-Pacific Niños connection: a multidecadal modulated mode', *Climate dynamics*, 43, 3163-3178.McGregor, S., Timmermann, A., Stuecker, M.F., England, M.H., Merrifield, M., Jin, F.F. and Chikamoto, Y. (2014) 'Recent walker circulation strengthening and pacific cooling amplified by atlantic warming', *Nature Climate Change*, 4, 888-892.Meehl, G.A., Arblaster, J.M., Fasullo, J.T., Hu, A. and Trenberth, K.E. (2011) 'Model-based evidence of deep-ocean heat uptake during surface-temperature hiatus periods', *Nature Climate Change*, 1(7), 360-364.Meehl, G.A., Gent, P.R., Arblaster, J.M., Otto-Bliesner, B.L., Brady, E.C. and Craig, A. (2001) 'Factors that affect the amplitude of El Nino in global coupled climate models', *Climate Dynamics*, 17, 515-526.Meehl, G.A., Hu, A., Castruccio, F., England, M.H., Bates, S.C., Danabasoglu, G., McGregor, S., Arblaster, J.M., Xie, S.P. and Rosenbloom, N. (2021) 'Atlantic and Pacific tropics connected by mutually interactive decadal-timescale processes', *Nature Geoscience*, 14, 36-42.Polo, I., Martin-Rey, M., Rodriguez-Fonseca, B., Kucharski, F. and Mechoso, C.R. (2014) 'Processes in the Pacific La Niña onset triggered by the Atlantic Niño', *Climate Dynamics*, 44, 115-131.Rodríguez-Fonseca, B., Polo, I., García-Serrano, J., Losada, T., Mohino, E., Mechoso, C.R. and Kucharski, F. (2009) 'Are Atlantic Niños enhancing Pacific ENSO events in recent decades?', *Geophysical Research Letters*, 36, L20705.Ruprich-Robert, Y., Msadek, R., Castruccio, F., Yeager, S., Delworth, T. and Danabasoglu, G. (2017) 'Assessing the Climate Impacts of the Observed Atlantic Multidecadal Variability Using the GFDL CM2.1 and NCAR CESM1 Global Coupled Models', *Journal of Climate*, 30(8), 2785-2810, available: .Ruprich-Robert, Y., Delworth, T., Msadek, R., Castruccio, F., Yeager, S. and Danabasoglu, G. (2018) 'Impacts of the Atlantic multidecadal variability on North American summer climate and heat waves', *Journal of Climate*, 31(9), 3679-3700.Ruprich-Robert, Y., Moreno-Chamarro, E., Levine, X., Bellucci, A., Cassou, C., Castruccio, F., Davini, P., Eade, R., Gastineau, G., Hermanson, L., Hodson, D., Lohmann, K., Lopez-Parages, J., Monerie, P.-A., Nicolì, D., Qasmi, S., Roberts, C.D., Sanchez-Gomez, E., Danabasoglu, G., Dunstone, N.,

Martin-Rey, M., Msadek, R., Robson, J., Smith, D. and Tourigny, E. (2021) 'Impacts of Atlantic multidecadal variability on the tropical Pacific: a multi-model study', *npj Climate and Atmospheric Science*, 4.Smith, T.M., Reynolds, R.W., Peterson, T.C. and Lawrimore, J. (2008) 'Improvements to NOAA's historical merged land–ocean surface temperature analysis (1880–2006)', *Journal of Climate*, 21(10), 2283-2296.Wang, B. and An, S. (2002) 'A mechanism for decadal changes of ENSO behavior: Roles of background wind changes', *Climate Dynamics*, 18(6), 475-486.Wang, G.J., Cai, W.J., Gan, B.L., Wu, L.X., Santoso, A., Lin, X.P., Chen, Z.H. and McPhaden, M.J. (2017) 'Continued increase of extreme El Nino frequency long after 1.5 degrees C warming stabilization', *Nature Climate Change*, 7(8), 568-572, available: .Wittenberg, A.T. (2009) 'Are historical records sufficient to constrain ENSO simulations?', *Geophysical Research Letters*, 36, L12702.Wu, X., Okumura, Y.M. and Dinezio, P.N. (2021) 'Predictability of El Niño duration based on the onset timing', *Journal of Climate*, 34, 1351-1366.Yu, J.Y., Kao, P.K., Paek, H., Hsu, H.H., Hung, C.W., Lu, M.M. and An, S.I. (2015) 'Linking emergence of the central Pacific El Niño to the Atlantic multidecadal oscillation', *Journal of Climate*, 28, 651-662.Zanchettin, D., Bothe, O., Graf, H.F., Omrani, N.E., Rubino, A. and Jungclaus, J.H. (2016) 'A decadally delayed response of the tropical Pacific to Atlantic multidecadal variability', *Geophysical Research Letters*, 43, 784-792.Zebiak, S.E. and Cane, M.A. (1987) 'A Model El Niñ–Southern Oscillation', *Monthly Weather Review*, 115, 2262-2278.Zhang, T., Shao, X. and Li, S. (2017) 'Impacts of atmospheric processes on ENSO asymmetry: A comparison between CESM1 and CCSM4', *Journal of Climate*, 30, 9743-9762.Zhang, W., Jiang, F., Stuecker, M.F., Jin, F.-F. and Timmermann, A. (2021) 'Spurious North Tropical Atlantic precursors to El Niño', *Nature communications*, 12(1), 1-8.

Geophysical Research Letters

Supporting Information for

Warm phase of AMV damps ENSO through weakened thermocline feedback

Paloma Trascasa-Castro[1], Yohan Ruprich-Robert[2], Frederic Castruccio[3], Amanda C. Maycock[1]

[1] School of Earth and Environment, University of Leeds, Leeds, UK

[2] Barcelona Supercomputing Center, Barcelona, Spain

[3] National Center for Atmospheric Research, Boulder, CO, USA

Contents of this file

- Figures S1 to S5
- Detailed methodology

Introduction

This document provides additional graphic information to support our results, including the sea surface temperature (SST) anomaly pattern associated with the positive phase of the Atlantic Multidecadal Variability (AMV) and El Niño Southern Oscillation (ENSO), a decomposition of the AMV modulation of ENSO feedbacks in its individual terms and an illustration of the linearity of the SW and β_h terms.

Additionally, this document contains detailed instructions to calculate the Bjerknes Stability index.

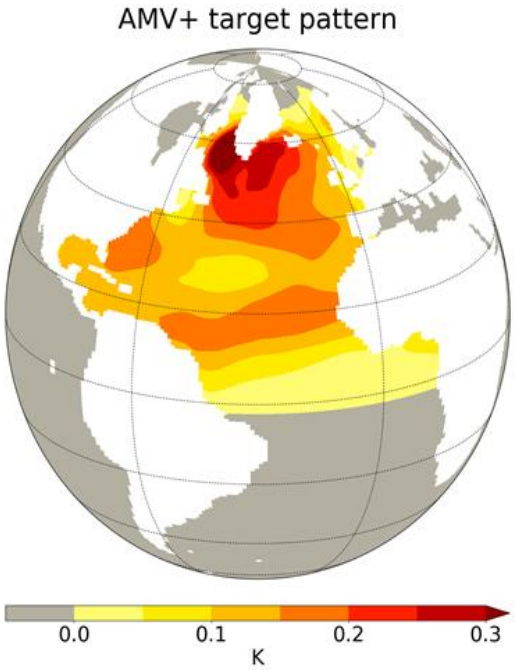

Figure S1. Target AMV+ sea surface temperature (SST) pattern. The AMV- is equivalent in amplitude but with opposite sign SST anomalies.

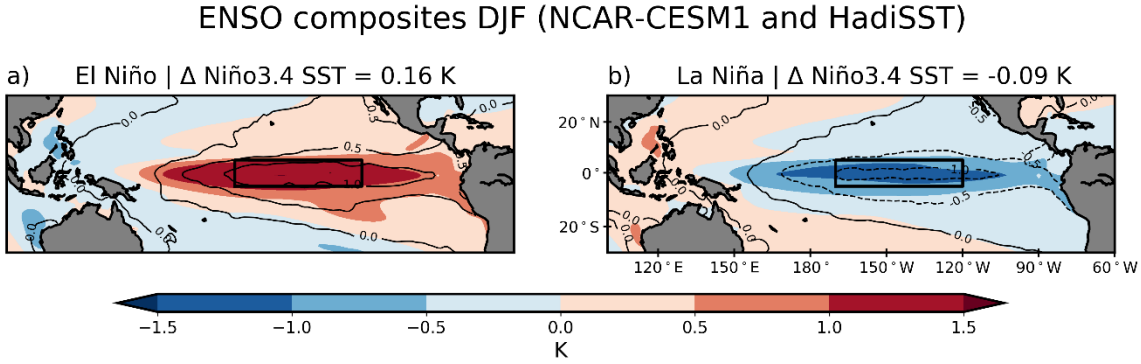

Figure S2. El Niño (a) and La Niña (b) SST anomaly composite in NCAR-CESM1 (filled contours) and observations (HadiSST, black contours). The differences in Niño3.4 SST anomalies between the model and observations is 0.16 K for El Niño and -0.09 for La Niña. The black rectangle denotes the Niño3.4 region (5°N-5°S, 170°E-120°E)

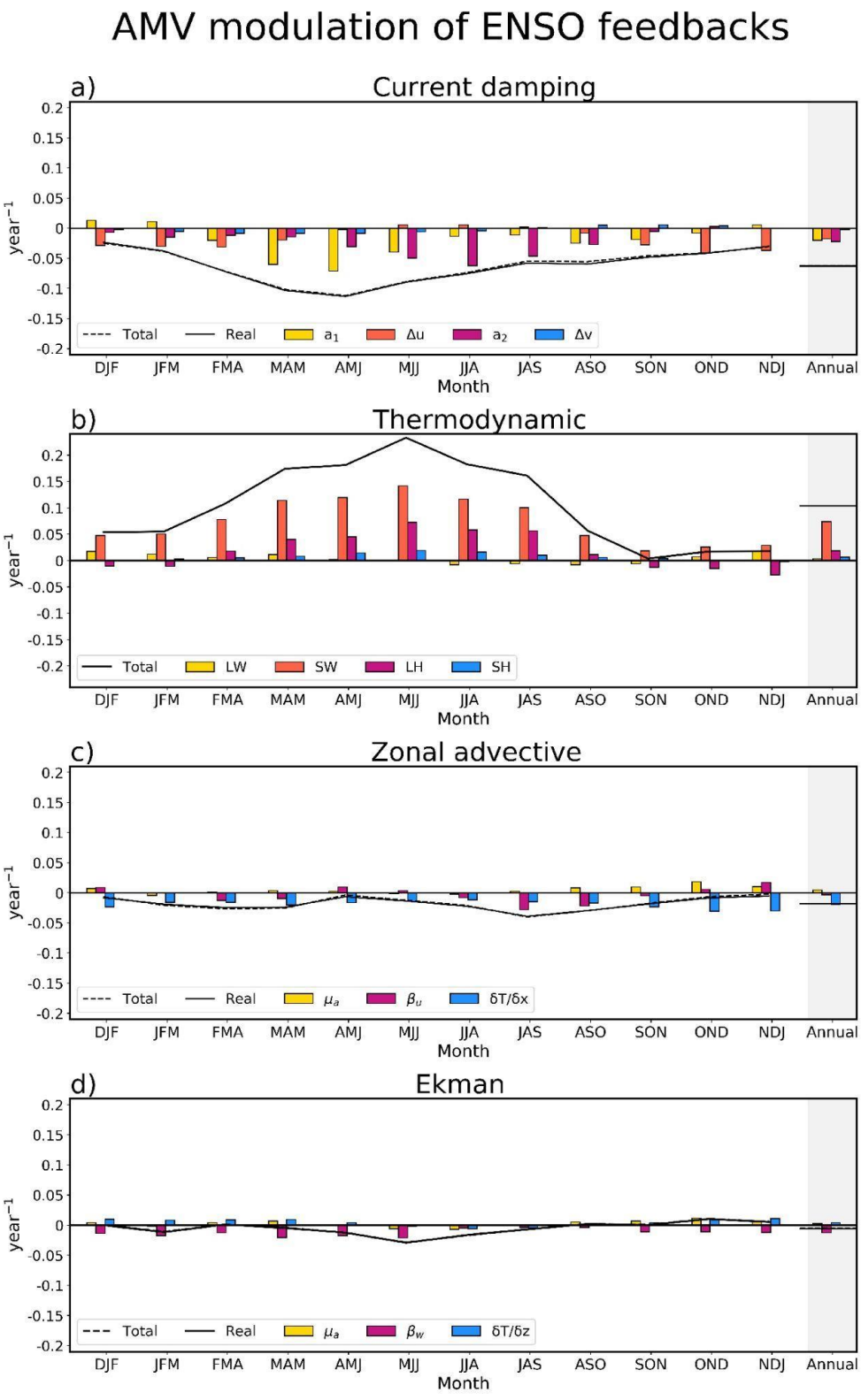

Figure S3. AMV modulation of the a) current damping, b) thermodynamic, c) zonal advective and d) Ekman feedbacks, decomposed onto their independent terms to homogenize their units. Monthly values are smoothed with a 3-month running mean.

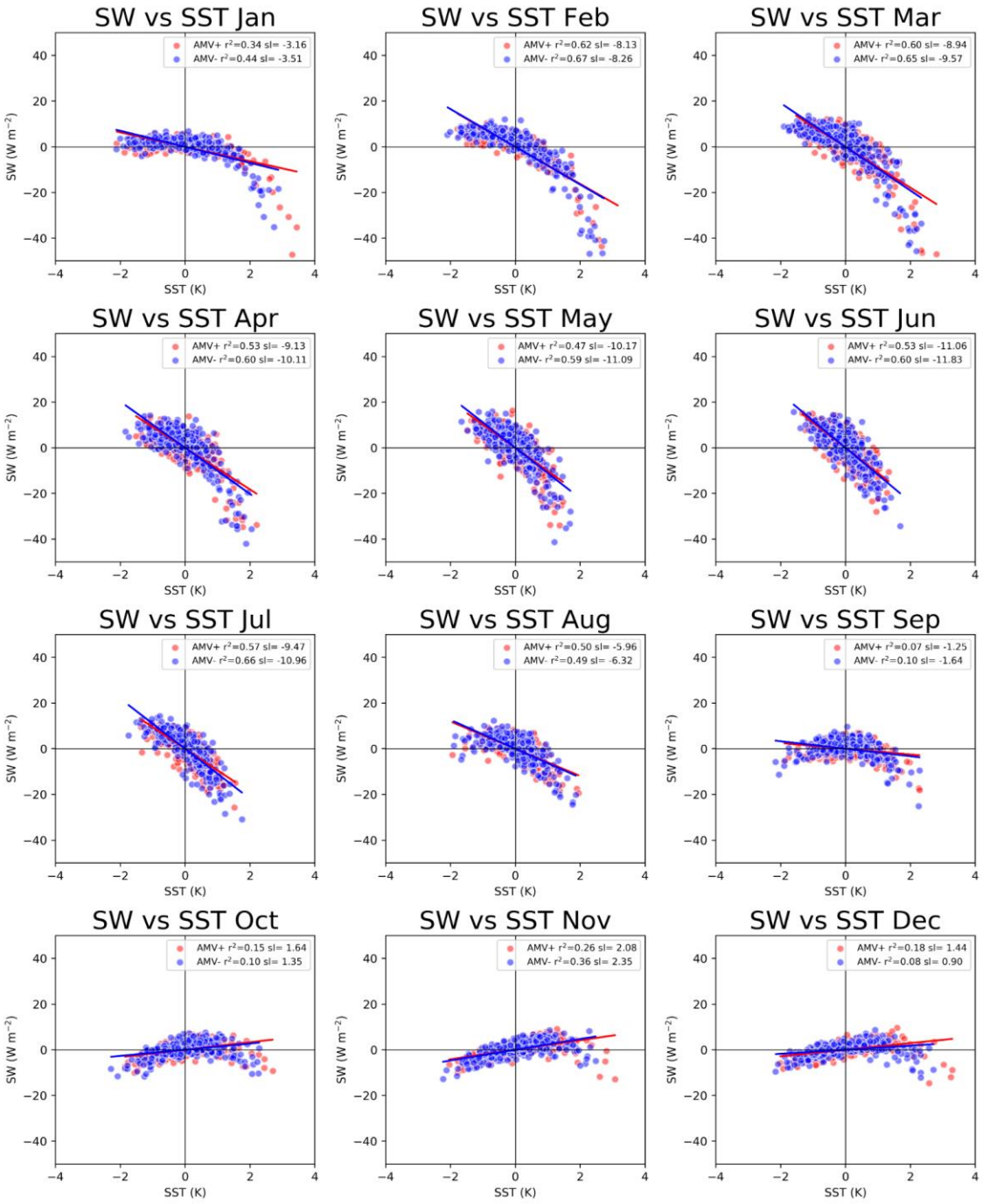

Figure S4. Scatterplot of monthly east Pacific shortwave radiation anomalies vs. east Pacific sea surface temperature anomalies in the AMV+ (red) and AMV- (blue) experiments. The legend shows the regression slope (W m^{-2} K^{-1}) and r^2 value.

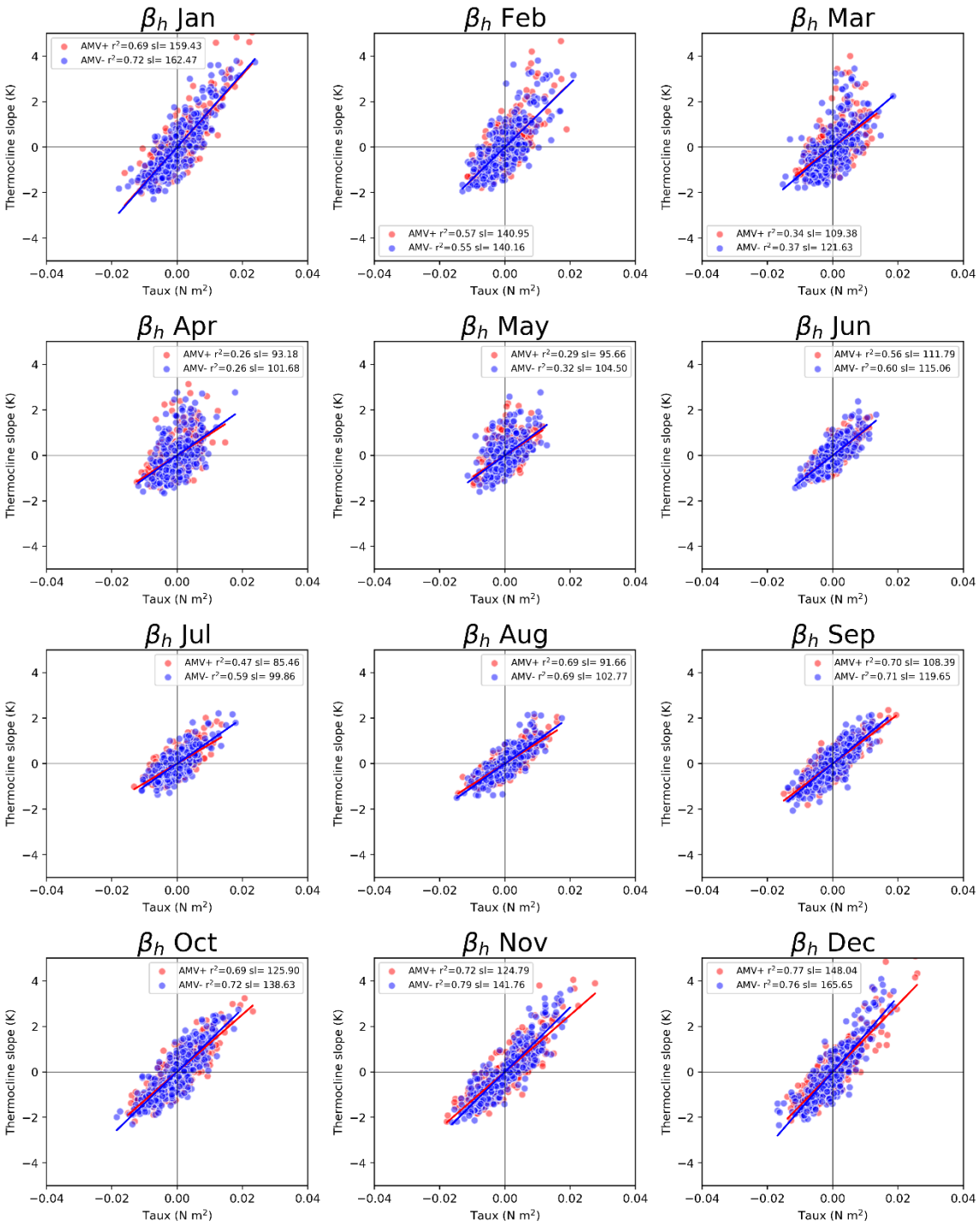

Figure S5. Scatterplot of monthly thermocline slope anomalies vs. equatorial Pacific wind stress anomalies in the AMV+ (red) and AMV- (blue) experiments. The legend shows the regression slope (K^{-1} $(N\ m^2)^{-1}$) and r^2 value.

Methodology to calculate the BJ index

$$2BJ = -\left[a_1 \frac{\langle \Delta\bar{u} \rangle_E}{L_x} + a_2 \frac{\langle \Delta\bar{v} \rangle_E}{L_y}\right]_{CD} - [\alpha_s]_{TD} + \left[\mu_a \beta_u \langle -\frac{\partial \overline{\mathrm{T}}}{\partial \mathrm{x}} \rangle_E\right]_{ZA} + \left[\mu_a \beta_w \langle -\frac{\partial \overline{\mathrm{T}}}{\partial \mathrm{z}} \rangle_E\right]_{EK} + \left[\mu_a \beta_h \langle -\frac{\bar{w}}{H_1} \rangle_E a_h\right]_{TC}$$

The Bjerknes Stability index (hereafter BJ index) is based on the recharge oscillator model (Jin 1997) and was introduced by Jin *et al*. (2006) with the aim of quantifying the different atmosphere and ocean mechanisms involved in ENSO growth rate.

The ENSO growth rate is estimated as the sum of, from left to right, the current damping (CD), thermodynamic (TD), zonal advective (ZA), Ekman (EK) and thermocline (TC) feedbacks. Following previous studies (Jin *et al.* 2006; Guilyardi *et al.* 2009; Kim and Jin 2011a; Kim and Jin 2011b; Kim *et al.* 2014; Lübbecke and Mcphaden 2014; An *et al.* 2017), the BJ index terms are calculated using linear regression between variables across all years in the simulations.

The boundary between the eastern and western Pacific is defined by regressing ocean heat content anomalies onto the timeseries of the first empirical orthogonal function (EOF) of anomalous SSTs. For the CESM1 model, the nodal line crosses the equator at 170°E, hence our eastern Pacific domain extends from 170°E to 80°W and from 5°N to 5°S. The equatorial Pacific domain has the same latitudinal boundaries that the EP region, but reaches 120°E on its western boundary.

1. Current damping

1.1 a_1

Linear regression of the SST difference between the western boundary of the eastern Pacific domain (i.e., averaged SST between 5ºS-5ºN at 170°E) and the eastern boundary of the domain (i.e., averaged SST between 5ºS-5ºN at 80°W) onto the mean SST of the eastern Pacific domain (i.e., averaged SST over 170°E-80°W / 5°N-5°S).

1.2 $\langle \Delta\bar{u} \rangle_E$

Difference of the climatological surface ocean zonal current between the western boundary of the East Pacific domain (5ºS-5ºN at 170°E) and the eastern boundary (5ºS-5ºN at 80°W). Units are m year^{-1}.

1.3 L_x and L_y

L_x is the longitudinal extent of the Eastern Pacific domain, in this case= 14,513,590 m.
L_y is the latitudinal extent = 2,480,797 m.

1.4 a_2

Linear regression of SSTs in the northern boundary of the Eastern Pacific box (5°N) minus SSTs in the southern boundary of the box (5°S) onto mean SSTs in the EP box (170°E-80°W, 5°N-5°S).

First of all, average SSTs between 170°E and 80°W, then extract SST values at the north and south locations and subtract N-S. Use absolute values, not anomalies. Units are K K^{-1}.

1.5 $\langle \Delta \overline{v} \rangle_E$

Climatological surface meridional ocean current difference between the northern boundary of the East Pacific box (5°N) minus southern boundary (5°S). Units are m $year^{-1}$.

2. Thermodynamic

Negative feedback. Longwave, shortwave, latent and sensible heat flux and SST anomalies are averaged over our East Pacific region. Then flux anomalies are regressed onto SST anomalies.

Units are in W m^{-2} K^{-1}, multiply by 0.14 to convert in $years^{-1}$ (Divide by the heat capacity of the water (4180 J kg^{-1} K^{-1}), the density of seawater (1029 kg m^{-3}) and the mixed layer depth (50 m), then multiply by 31,536,000 to convert from $seconds^{-1}$ to $year^{-1}$).

3. Zonal advective

3.1 μ_a

Equatorial Pacific (120°E - 80°W, 5°N - 5°S) wind stress anomalies regressed onto East Pacific (170°E - 80°W, 5°N - 5°S) SST anomalies. Units are 10^{-3} N $m^{-2}K^{-1}$. Area averaged before regression.

3.2 β_u

Regression of EP (170°E - 80°W, 5°N - 5°S) ocean surface zonal current anomalies (10^{-2} m s^{-1}) against equatorial Pacific (120°E - 80°W, 5°N - 5°S) (10-3N m^{-2}). Units are in seconds, multiply by 31,536,000 to get units of $year^{-1}$. Area averaged before regression.

3.3 $\langle -\frac{\partial \overline{T}}{\partial x} \rangle_E$

Mean zonal SST gradient over EP (170°E - 80°W, 5°N - 5°S). Use climatological SSTs, not anomalies.

4. Ekman

See zonal advective feedback for the definition of μ_a

4.1 β_w

Regression of EP (170°E - 80°W) upwelling ocean current anomalies (10^{-2} m s^{-1}): Average values from 0-50m against equatorial Pacific (120°E and 80°W) surface wind stress anomalies (10^{-3}N m^{-2}).

4.2 $\langle -\frac{\partial \overline{T}}{\partial z} \rangle_E$

Mean vertical temperature gradient over EP (average 170°E - 80°W, 5°N - 5°S) from 0 to 50m depth. Use climatological SSTs, not anomalies.

5. Thermocline

See zonal advective feedback for the definition of μ_a

5.1 β_h

Regression of thermocline slope anomalies =difference between EP (170°E - 80°W) and WP (120°E - 170°E) ocean temperatures averaged from the surface to 300m against equatorial Pacific (120°E - 80°W) surface wind stress anomalies.

5.2 $\langle -\frac{\overline{w}}{H_1} \rangle_E$

Climatological upwelling values over the East Pacific (170°E - 80°W) divided by 50 m. Negative w set to 0 instead of masking.

5.3. a_h

Upper ocean heat content (temperatures averaged from 0 to 300m) anomalies in the East Pacific regressed onto temperature anomalies at 50m depth, accounting only for upwelling.

References

An, S.I., Heo, E.S. and Kim, S.T. (2017) 'Feedback process responsible for intermodel diversity of ENSO variability', *Geophysical Research Letters*, 44, 4272-4279.

Guilyardi, E., Braconnot, P., Jin, F.F., Kim, S.T., Kolasinski, M., Li, T. and Musat, I. (2009) 'Atmosphere feedbacks during ENSO in a coupled GCM with a modified atmospheric convection scheme', *Journal of Climate*, 22, 5698-5718.

Jin, F.-F. (1997) 'An Equatorial Ocean Recharge Paradigm for ENSO. Part I: Conceptual Model', *Journal of the Atmospheric Sciences*, 54, 811-829.

Jin, F.F., Kim, S.T. and Bejarano, L. (2006) 'A coupled-stability index for ENSO', *Geophysical Research Letters*, 33.

Kim, S.T., Cai, W., Jin, F.F. and Yu, J.Y. (2014) 'ENSO stability in coupled climate models and its association with mean state', *Climate Dynamics*, 42, 3313-3321.

Kim, S.T. and Jin, F.F. (2011a) 'An ENSO stability analysis. Part I: Results from a hybrid coupled model', *Climate Dynamics*, 36, 1593-1607.

Kim, S.T. and Jin, F.F. (2011b) 'An ENSO stability analysis. Part II: Results from the twentieth and twenty-first century simulations of the CMIP3 models', *Climate Dynamics*, 36, 1609-1627.

Lübbecke, J.F. and Mcphaden, M.J. (2014) 'Assessing the twenty-first-century shift in enso variability in terms of the bjerknes stability index', *Journal of Climate*, 27, 2577-2587.